Diamond & Related Materials 96 (2019) 58–66

Contents lists available at ScienceDirect

Diamond & Related Materials

journal homepage: www.elsevier.com/locate/diamond

Effect of chemical activation on the cellular structure of biopitch-derived green carbon foam

Adife Seyda Yargic*, Nurgul Ozbay

Chemical Engineering Department, Engineering Faculty, Gulumbe Campus, Bilecik Seyh Edebali University, 11210 Bilecik, Turkey

ARTICLE INFO

Keywords:
Biopitch
Carbon foam
Chemical activation
Pyrolysis tar
Spruce tree sawdust

ABSTRACT

Current researches pay particular attention to cost-effective and abundant raw materials such as biomass as an alternative to fossil-derived-carbonaceous precursors. The aim of this study is to examine the usability of pyrolytic oil as a biopitch source in the foaming process and to investigate the effect of chemical activation on the characteristics of carbon foam. The elemental analysis of the biopitch supported the fact that the H/C and O/C ratios of wood-tar-based-pitch had high oxygenated and aliphatic carbons in contrast to fossil-pitches. Various basic analysis methods such as elemental analysis, X-ray diffraction, nitrogen sorption isotherms, Raman spectroscopy, scanning and transmission electron microscopy, true/bulk density and compressive strength tests were applied to analyze carbon foams. When the results of nitrogen sorption analysis were examined, it was determined that the surface area of carbon foam increased to about 31 times after activation. According to the pore size distribution graphs, the foams had regular pore distribution; additionally, the pore size in the mesopore region was determined to shift to the micropore region with activation. Compressive strength values were in the range of 0.40–1.97 MPa. Moreover, an increase in porosity values and a decrease in compressive strength values were observed due to enhancing porosity as a result of the activation process.

1. Introduction

Advanced carbonaceous materials (ACMs) are attracting worldwide attention due to their special microstructures, unique properties and potential applications in various fields. In order to develop competitive carbonaceous materials, it is necessary to take into account the production of them from renewable sources [1]. Carbon foams, one of the advanced carbonaceous materials, are classified into two categories as graphitic carbon foams and non-graphitic carbon foams according to parameters such as precursor and heat treatment used during preparation. Graphitic foams are prepared by the application of carbonization and graphitization treatments to coal, coal tar pitch and petroleum pitch after foaming [2]. On the other hand, non-graphitic (amorphous) carbon foams are synthesized from synthetic polymers, natural products such as sucrose or tannin, or oxygenated precursors, and high amounts of pyrolysis carbon residues are formed [3]. Non-graphitic foams, which are usually derived from thermoset polymer foams, exhibit low thermal and electrical conductivity. The precursors of such non-graphitic foams are listed as formaldehyde-cross-linked phenol or resorcinol, polyurethane, furfural resin, polyvinyl chloride [4]. The cavity volumes in carbon foams are controlled by the porosity which provides the linkage between pores and the outer surface of the foam. Foams with the hollow structure are called as “open-celled” or “porous.” Else, materials without internal cavity volumes or with cavities that do not come into contact with the exterior of the material are defined as “closed cell” or “nonporous” materials [5].

When pyrolysis or carbonization of hardwoods, such as beech, birchwood or ash tree, is carried out, tar is formed beside gas and light liquid products in a yield of about 10% by weight. Wood tar is a complex mixture consisting essentially of phenols, acids, aldehydes, and ketones [6,7]. Since the main components of tar are phenols, they can be applied as a carbon source [8]. In chemical process industries, the black or dark brown residue produced by distillation of coal tar, wood tar, oils, fatty acids or stationary oils is defined as “pitch”. Wood tar is fractionated to separate fine chemicals such as phenyl, guaiacyl and syringyl derivatives. The solid residue of wood tar distillation (about 50% depending on distillation conditions) is called as “wood tar pitch” or “biopitch” and is used as a precursor for polymeric materials [6,9].

ACMs, which have relevant specific properties for various applications, consist essentially of carbon in terms of chemical content. The studies are concentrated on fossil pitches (coal tar and petroleum pitches), which have great potential as ACM precursors [10–12]. ACM production using pitch is very important when considering economic and technological aspects. This is because of the possibility of obtaining

* Corresponding author.
E-mail address: seyda.guler@bilecik.edu.tr (A.S. Yargic).

https://doi.org/10.1016/j.diamond.2019.04.032
Received 5 February 2019; Received in revised form 22 April 2019; Accepted 27 April 2019
Available online 06 May 2019

materials that can be used in many applications from abundant and cheap raw materials [9,13,14].

However, it has been determined that there is not much work with wood tar pitch as the precursor of the ACM. In Brazil, pyrolytic oil is used, which is evolved by the slow pyrolysis of eucalyptus as a result of coal production [9]. Recently, some polymeric materials in the biopitch have been synthesized to obtain advanced carbon materials [9,15,16] and phenolic resins [17]. Biopitch is also used as the polyol in polyurethane elastomers, as composite and coating material. Since biopitch can be used as a source of renewable polyols, the pitches, which are the distillation residue of the tars obtained in the process of producing eucalyptus coal, are used in order to investigate the effect of the biopitch on the properties of flexible polyurethane foams [6]. At this point, the aim of the study was to highlight the importance of the utilization of biopitch produced from a renewable industrial waste source as an alternative to fossil pitches in the production of valuable carbon foam material. As commonly done in terms of agricultural and forested areas rich in Turkey, a considerable amount of waste biomass is released. When carbon foams are produced with the desired properties by using these wastes, it is thought that this research will contribute to the studies in this area. In this respect, biopitch was produced from pyrolysis tars of spruce tree sawdust with high lignin content by vacuum distillation method and used as carbon foam precursor in high temperature/pressure reactor. The lignin content of the precursor yields to a great quantity of phenolic tar which can be used in the production of the pitch with tunable mesophase properties. Besides, the structures of the foams produced in the high temperature/pressure reactor were investigated by means of potassium hydroxide activation. The structural properties of carbon foams were examined by several characterization techniques.

2. Experimental

2.1. Biomass feedstock

The waste sample of spruce tree sawdust (*STS*) examined in this study was taken from a wood processing factory in Eskişehir (Turkey), and then it was air-dried in the laboratory. The particle size of *STS* was reduced by using a grinder (Armfield FT-7A) and precursor was sieved for the suitable particle diameter range of $0.425 > Dp > 0.25$ mm. Mean particle size was specified as 0.75 mm. The structural and preliminary analyses were carried out for proximate analysis of *STS* by using ASTM standard test methods [5]. Holocellulose, hemicellulose, cellulose and lignin contents were extractive free basis; and the volatile matter content was 78.61% while ash content was 1.41%. According to its high volatile and low-ash content, spruce tree sawdust is a suitable biomass feedstock for the pyrolysis process. Carbon, hydrogen, nitrogen, and oxygen contents were clarified to accomplish an ultimate analysis of *STS* via Elemental Analyzer (Leco CNH628 S628) by using helium, dry air, and oxygen gases. The complete combustion of all organic samples was carried out by operating Elemental Analyzer's furnace at 950 °C. The oxygen content was calculated as the difference between 100 and the total wt% of CHN constituents. The carbon content of *STS* was found as 46.55 wt% and lignin content was 35.21 wt% which were important for biopitch and carbon foam production. The calorific value of feedstock was calculated as 19.20 MJ/kg due to ultimate analysis results using Dulong's formula as reported by Harker and Backhurst [18].

2.2. Pyrolysis of STS and pyrolytic oil production

Stainless steel (#316) fixed-bed Heinze retort was used to perform pyrolysis experiments under a static atmosphere without any sweeping gas. The reactor was heated externally by an electrical furnace in which the temperature was controlled by a thermocouple inside the bed. *STS* (15 g) was placed in the reactor and the temperature was raised to the final temperature of 400 °C with 7 °C/min heating rate and held for a minimum of 20 min until no further significant release of gas was observed. The liquid products condensed in collecting bottles maintained at about 0 °C were recovered by washing with dichloromethane. Aqueous and bio-oil phases of the liquid product were separated from each other with a separating funnel. Bio-oil and solvent mixture was passed over anhydrous sodium sulfate to make it water free; then the solvent was evaporated with a rotary evaporator. The solid product was taken out of the reactor, weighed as char. Char yields were determined from the overall weight losses of the reactor. The amount of gaseous products was calculated by subtraction of solid, liquid and water yields from the amount of initial *STS*. The yield of liquid product was 19.05% at 400 °C, and the solid product was obtained with a yield of 30.25%. The remaining part was pyrolytic liquid, the content of which was 29.02% water and 21.68% bio-oil.

2.3. Fabrication of biopitch via pyrolysis of precursor

In order to prepare carbon foam using biopitch, the acidic water phase was separated from the bio-oil obtained as a result of pyrolysis experiments at 400 °C. Subsequently, the biopitch was produced from the aromatic structures in the heavy phase via the vacuum distillation apparatus. It is known that the selected temperature of 360 °C for producing coal tar and petroleum pitches is very high for bio-oils and the 270 °C temperature can be used as the highest temperature. When the temperature exceeds 270 °C, the bio-oil rapidly reacts to form a solid thermofix carbonaceous residue. It is indicated that this high reactivity is attributed to high oxygen content (about 20%) in bio-oil, and the oxygen content of fossil pitches is very low (about 2%) [19]. According to the preliminary studies, it was decided to use the biopitch produced at distillation time of 24 h at 250 °C in 50 mbar vacuum pressure for carbon foam production. The structure of biopitch was investigated by ash content determination, elemental analysis, helium gas pycnometer, thermogravimetric analysis, and Fourier transform infrared spectrometry techniques.

2.4. Foaming process, activation, and characterization of carbon foams

The biopitch powders were put inside a cylindrical aluminum mold for the foam production. The foaming process of carbon foam derived from biopitch (*BPCF*) was carried out in a Parr reactor (Parr Instrument Company, USA). The reactor was purged with nitrogen to ensure an inert atmosphere and operated at 1 MPa. The reactor was heated with a heating rate of 2.5 °C/min up to 450 °C and soaked for 1 h. Finally, the reactor pressure was released to atmospheric pressure and left to cool down to room temperature to attain the green pitch foams. The schematic diagram of carbon foam processing was illustrated in Fig. 1.

The green carbon foam was chemically activated with potassium hydroxide (KOH) in order to increase the surface area. For this purpose, the green foam was treated with KOH such that the impregnation ratio was 1:1 for the activation agent:foam, then it was carbonized at 1050 °C. When potassium hydroxide is used; chemical reactions between the activation agent and the foam cause an increase in the surface area during the heat treatment. The reaction between carbon and KOH actuates as a solid-solid phase reaction and continues as a solid-liquid reaction. In this case, the potassium source is reduced to form K metal, carbon is oxidized to carbon oxide and carbonates, and other reactions between the various active intermediates occurs [20]. Both KOH and K_2CO_3 react with the carbon in the foam structure and form metallic potassium. Furthermore, carbon monoxide gas is formed by the decomposition of K_2CO_3, and the resulting gas serves as the second activation agent during the depolymerization reactions. The redox reaction between carbon and KOH and other possible reactions are defined in Eqs. (1)–(9) [21,22].

$$6KOH + 2C \rightarrow 2K + 3H_2 + 2K_2CO_3 \quad (1)$$

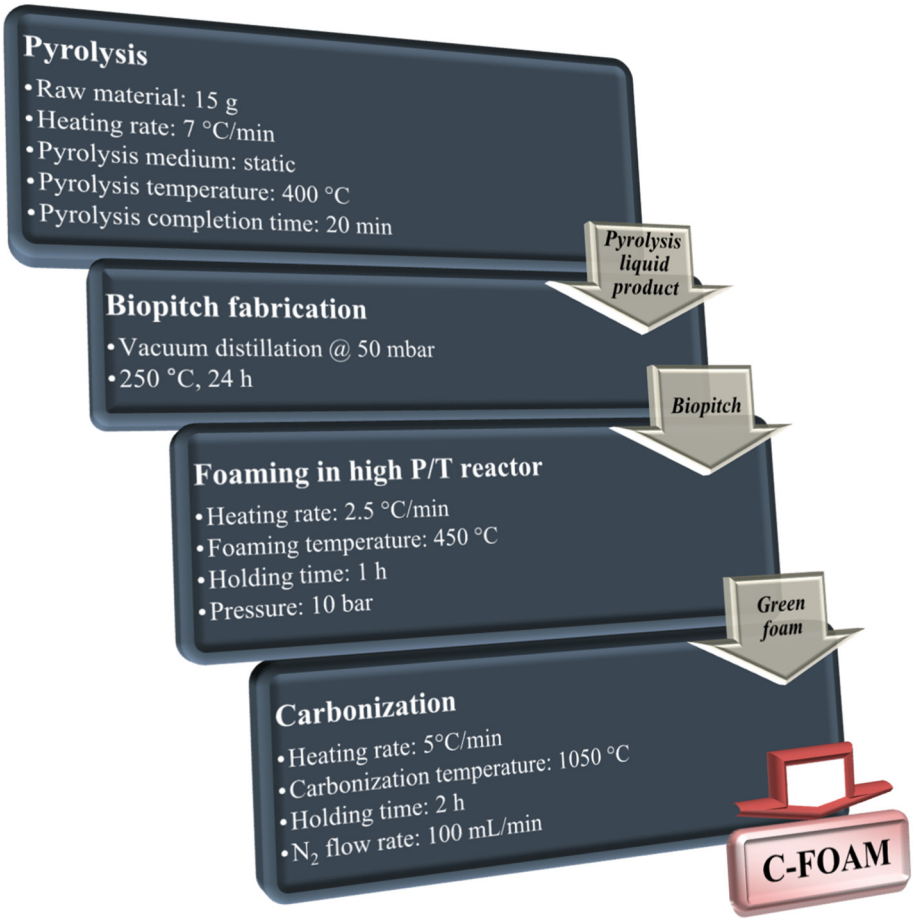

Fig. 1. The schematic diagram of carbon foam processing.

$$2KOH \rightarrow K_2O + H_2O \quad (2)$$

$$K_2CO_3 \rightarrow K_2O + CO_2 \quad (3)$$

$$K_2CO_3 + 2C \leftrightarrow 2K + 3CO \quad (4)$$

$$K_2O + H_2 \rightarrow 2K + H_2O \quad (5)$$

$$K_2O + C \rightarrow 2K + CO \quad (6)$$

$$C + H_2O \rightarrow CO + H_2 \quad (7)$$

$$CO + H_2O \rightarrow CO_2 + H_2 \quad (8)$$

$$CO_2 + C \rightarrow 2CO \quad (9)$$

In the literature, it is concluded that the reactions occurring during the activation of various carbon sources with KOH are mainly based on three mechanisms; the formation of the pore network by *i)* chemical activation (Eqs. (1), (4), (6)) and *ii)* physical activation (Eqs. (2), (3), (5), (7)–(9)), and *iii)* intercalating of metallic K into the carbon matrix and expansion of the carbon lattices [20,23].

The resultant green foams (as-synthesized or activated) were transferred to carbonization furnace and heated to 1050 °C with 5 °C/min heating rate under a nitrogen atmosphere for 2 h. The carbonized foams were respectively denoted as BPCF and BPAF according to the state of being as-synthesized or activated. The intrinsic characteristics of the foam sample (crystal properties, cell structure, and microstructure difference) were evaluated by X-ray diffraction (PANalytical X'Pert Pro Materials Research Diffractometer employing CuKα radiation (λ = 0.15406 nm, in the range of 0–80° 2θ)), SEM observation (Zeiss Supra VP 40) with platinum sputter-coated (Quorum Q 150 R ES DC Sputter), TEM (JEOL 1220 JEM, 80 keV) textural analysis, nitrogen sorption (Micromeritics ASAP 2020 instrument at 77 K), and confocal Raman spectrum (RENISHAW Raman Spectrometer operating with an excitation wavelength of 532 nm and power of 0.5 mW), respectively. Besides that, compressive strength measurements were carried out with Shimadzu AG-IC 100KN with 0.5 mm/min loading rate. The bulk density of the carbon foam was calculated by weighing foam with known dimensions, and true density was measured by Micromeritics, Accupyc II 1340.

3. Results and discussion

3.1. Biopitch properties

CHN and ash contents, % yield, softening point, true density, acetone- and toluene-insoluble fractions of biopitch (L-P50-250 °C-24 h) were given in Table 1. According to Table 1, the biopitch was produced about 17% yield at 250 °C and 50 mbar vacuum pressure after 24 h

Table 1
Biopitch properties (T = 250 °C, P = 50 mbar, t = 24 h).

Precursor	*STS* bio-pitch
C (%)	73.760
H (%)	6.665
O (%)	18.657
N (%)	0.918
Pitch yield (%)	16.79
Ash (%)	0.049
Density (g/cm^3)	1.20
AI (%)	28.2
TI (%)	22.3
SP (°C)	118.7

Table 2
The characteristics of the different pitches in the literature.

Pitch type	C (%)	H (%)	O (%)	N (%)	Ash (%)	Density (g/cm^3)	SP (°C)	Reference
Coal tar pitch	90.90	4.95	2.75	0.90	–	–	–	[24]
Coal tar pitch	93.28	4.17	1.08	0.96	–	–	116.0	[25]
Coal tar pitch	–	–	–	–	0.001	1.28	86.6	[26]
Coal tar pitch	90.60	5.25	2.75	0.90	–	–	72	[27]
Coal tar pitch (H_2SO_4)	83.90	4.24	8.42	0.82	–	–	140	[27]
Coal tar pitch (350 °C, H_2SO_4)	91.20	3.83	2.05	0.80	–	–	280	[27]
Mesophase pitch	–	–	–	–	0.05	1.32	232	[26]
Mitsubishi AR24 pitch	93.90	5.23	0.43	0.38	–	–	237	[28]
Petroleum pitch	93.01	6.03	0.84	0.05			111.0	[25]
Petroleum pitch	91.90	5.39	0.82	0.19	< 0.10	–	127.0	[29]
Eucalyptus biopitch (250 °C, 4 h)	71.60	6.00	21.30	–	1.1	–	112.0	[30]
Eucalyptus biopitch (150 °C, 4 h, $AlCl_3$)	69.80	6.20	21.60	–	2.4	–	103	[30]
Eucalyptus biopitch (150 °C, 4 h, CH_2O)	68.50	6.50	23.4	–	1.5	–	134	[30]
Eucalyptus biopitch (270 °C, 0.1 MPa)	70.50	6.30	22.60	0.60	0.20	–	108.0	[19]

distillation and had a softening point above 100 °C (118.7 °C). Since the ash content of precursor (1.41%) was low, it was determined that the content of ash in biopitch was low. As the ash content was < 1%, it was accepted at the negligible level. The true density of the biopitch was measured to be 1.20 g/cm^3 based on the helium gas pycnometry analysis. In addition, 22.3% of toluene-insoluble (TI%) and 28.2% of acetone-insoluble (AI%) fractions were determined. The acetone-insoluble fraction is a term related to the degree of polymerization of the biopitch. The solubility of fossil pitches is usually determined by toluene- and quinolone-insoluble fractions (TI and QI). Since wood tar pitches are almost completely soluble in these solvents, it has been reported that the use of acetone in the analysis of these materials is more appropriate. The reduction of pitch solubility in acetone is due to a decrease in the configurational entropy of the mixture during polymerization. As the softening point rises, the increase in the acetone-insoluble fraction indicates that the degree of polymerization has increased [9]. The characteristics of the different pitches in the literature were given in Table 2 in order to compare the produced biopitch. Although the C content of the *STS*-based pitch was lower than the coal- and petroleum-based pitches, it was higher than the biomass-based pitches. The softening point of the *STS*-based biopitch and the other pitches used in the production of carbon foam were determined to be in harmony.

FT-IR analysis was performed to determine the functional groups in the structure of the biopitch. According to the FT-IR spectra shown in Supplementary Data (SD.1), the biopitch were found to have a complex structure and contain similar functional groups of lignin structure [31]. Characteristic absorption bands of aliphatic and aromatic hydrocarbons, phenols, ethers, esters, and ketones were observed in the structure of biopitch which had thermoplastic behavior and macromolecular framework. The presence of these functional groups was consistent with H/C ratios based on the elemental analysis results.

The functional groups in the FT-IR spectra were given in Table 3 [32]. A strong absorption band of free phenolic −OH and −COOH groups was observed in the range of 3600–3200 cm^{-1}. Two carbonyl bands observed around 1700 cm^{-1} supported the presence of carboxylic acids and ketones. Peaks indicating aromatic structures were observed at the range of 1600–1400 cm^{-1}, ether and phenolic −OH groups in the structure were found in the range of 1200–1100 cm^{-1} [6,33]. The carbonyl group and ether bonds observed around 1700 and 1100 cm^{-1} demonstrated the presence of guaiacyl and syringyl units in the structure [34].

The thermogravimetric analysis of the biopitch under the nitrogen atmosphere was investigated to determine the working temperature in the high temperature/pressure reactor (Fig. 2). When TG results were examined, it was seen that the biopitch consistently degraded at a temperature of 200–420 °C and the weight loss was ~66%. This behavior can be explained by the high oxygenation standard (18.66% O) in biopitch. During pyrolysis, oxygen in the three-dimensional chain of the pitch was released and promoted self-combustion. This also depended on the high aromaticity of the pitch structure [32]. In the thermogravimetric analysis, it was determined that the biopitch had a residual carbon content of 39% when it was heated to a foaming temperature of 450 °C.

3.2. Carbon foam characterization

Examination of the structural properties and surface morphology to determine the application area of the carbon foam is particularly important.

3.2.1. Elemental analysis

The results of the elemental analysis of BPCF and BPAF were given in Table 4. Carbon foams were produced with 83–89% carbon and 9–15% oxygen contents. It was determined that the carbon content of the carbon foams obtained after the activation process using potassium hydroxide decreased and the oxygen content increased from 9.042% to 15.012%. The yield of carbon foam produced from biopitch was calculated as 41.58%.

3.2.2. SEM and TEM analysis

SEM images of the carbon foams produced in the high temperature/

Table 3
Functional groups in the structure of the biopitch.

L-P50-250 °C-24 h	Wavenumber (1/cm)	Functional group
3445	3450	OH (alcohol, phenol) and NH (amine) stretching band
2900	3030–2850	CH alkane stretching band
2100	2270–2100	C≡CH alkyne stretching band
1685	1770–1650	Nonconjugated C═O (aldehyde, ketone, carboxylic acid) stretching band
1600	1650–1450	C═C_{ar} (aromatic) stretching band
1120	1115	CH bending band of the guaiacyl and syringyl
745	730	C═C cis bending band

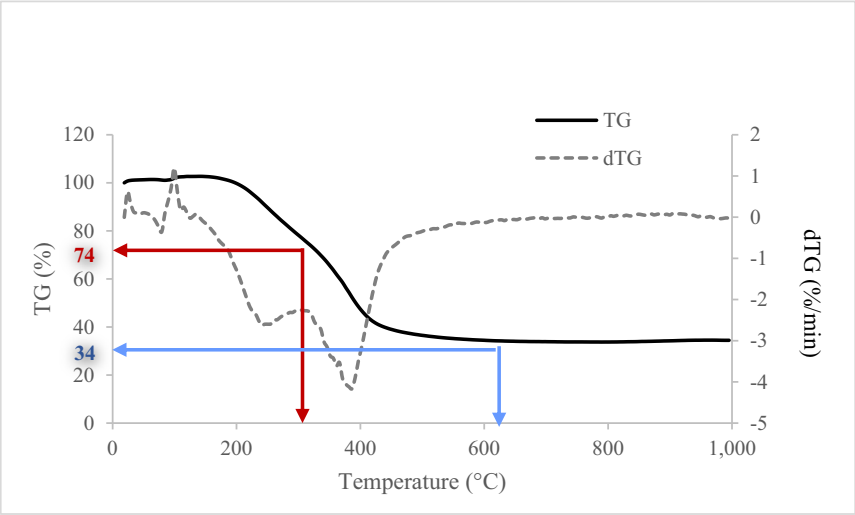

Fig. 2. TG and DTG curves of biopitch (L-P50-250 °C-24 h) under a nitrogen atmosphere.

Table 4
Elemental analysis of carbon foams produced at 450 °C and 10 bar.

Foam	C (%)	H (%)	O (%)	N (%)
BPCF	89.040	0.486	9.042	1.432
BPAF	83.267	0.589	15.012	1.132

pressure reactor were shown in Fig. 3a and b. According to the SEM images, the cell size and cell distribution in the foams were similar, and the foams had a closed-cell structure. As a result of activation with potassium hydroxide, it was determined that cracks occurred in the cell walls and the pores were opened. In the structure of carbon foams, various cells sizes were found in the range of 50–400 μm. TEM images of as-synthesized and KOH-activated carbon foams were given in Fig. 3c and d. Both carbon foams also appeared to have the multilayer structure of graphene. However, it has been determined that the structure of the carbon foam activated with KOH (BPAF) had a more regular pore structure than the as-synthesized carbon foam (BPCF). The TEM and SEM images corroborated the nitrogen sorption and x-ray diffraction analysis results.

SEM images of the produced foams were found to be compatible with SEM images of carbon foams obtained using coal tar pitch and Mitsubishi AR mesophase pitch [35–38]. One of the important

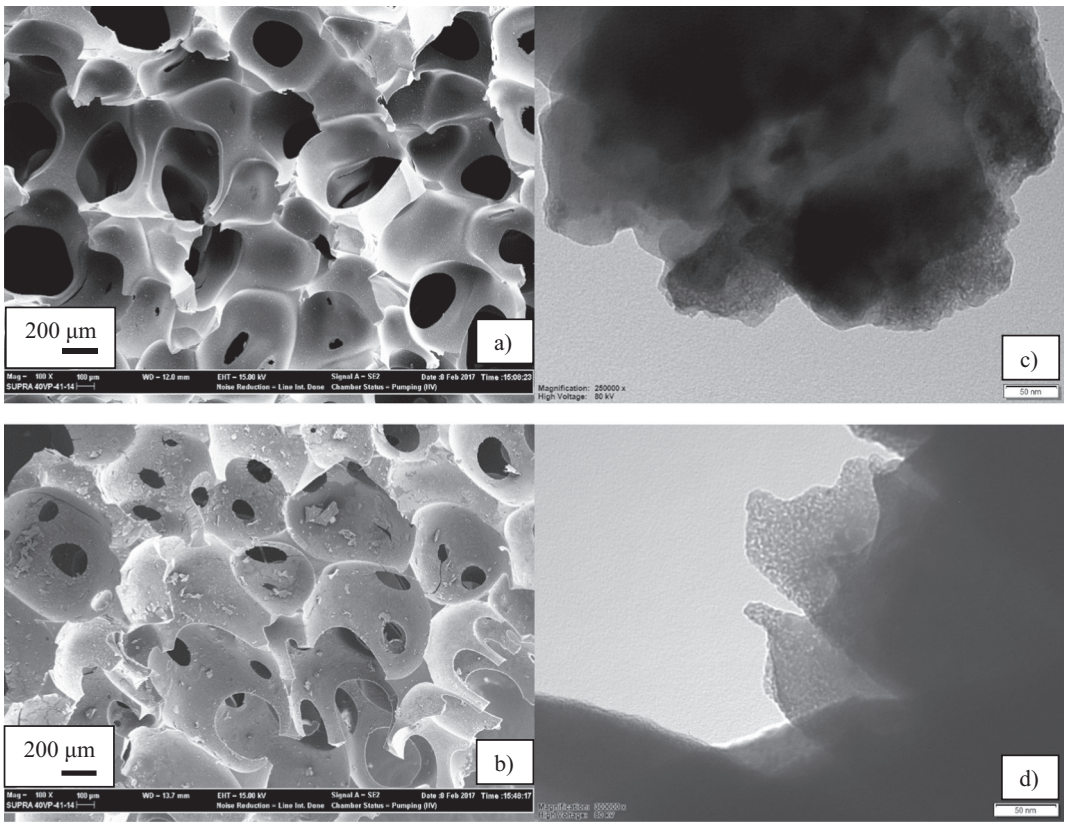

Fig. 3. SEM (a and b) and TEM (c and d) images of carbon foams: (a and c) as-synthesized (BPCF), (b and d) activated (BPAF) foams.

properties of carbon materials is that they have a wide range of pore structure in various sizes, morphology and pore content. Porous carbon foams (micro-, meso- or macro-) prepared through different processes attract the attention of scientists and engineers. Carbonaceous materials can have various morphologies including fibrous, tubular, spherical, flat granular and granular. Among them, the carbon foam has a special pore structure with interconnected macro-pores (cells), i.e., its open cell structure. Depending on this cell structure, they have new properties such as wide geometric surface area and basic properties of carbonaceous materials such as lightness, high thermal stability, hydrophobic surface, high thermal and electrical conductivity. It is possible to change the thermal and electrical conductivity of the bulk carbon materials by controlling *i)* the regularity or irregularity of the nanostructures, and *ii)* graphitic or amorphous structures. According to the terminology used to characterize carbon foams, a macro-pore in the structure was called as a cell surrounded by carbon wall. Meso- and micro-pores are also located on the carbon wall [39].

3.2.3. XRD analysis

The atomic and molecular structures of crystalline materials are identified via X-ray diffraction analysis technique which is similarly critical for graphene-like materials. X-ray diffraction patterns of carbon foams were shown in Fig. 4, while XRD parameters were shown in Table 5. Two main planes of (1 0 0) and (0 0 2) are the characteristics of carbon-based materials. The reflection of (1 0 0) and (1 0 1) detected at 2θ = 41–45° is a typical reflection of the 2D arrangement of C-layers in graphite-like materials. 2θ values of 22°, 25°, 26°, and 31° are detected for identifying graphene layers with disordered stacking, hexagonal carbon, hexagonal and orthorhombic graphite, respectively [5]. Besides, the 2θ value of 44° is the sign of (1 0 0) plane of graphene layers with disordered stacking. The sharp (0 0 2) diffraction peak indicates a highly graphitic ordered structure of graphene multilayers [40]. Commonly, 10°-30° range is investigated for the notification a wide band stacked graphitic basal plane for all carbonaceous materials, in which the maximum value of ~2θ = 25° is the sign of the (0 0 2) peak [5]. The characteristic peaks are in accordance with the standard Joint Committee on Powder Diffraction Standards (JCPDS) card numbers of 98-061-7290, 98-002-9123, 98-008-8811/8812, 98-005-3781.

Graphite is a form of carbon in which the atoms are covalently bonded (sp^2) together in layers of hexagonal rings joined together. In graphite structure, further carbon-carbon bonds extend out of each ring to link with other rings [41]. In the graphite structure, the layers of carbon hexagons are stacked in parallel. The thermodynamically stable

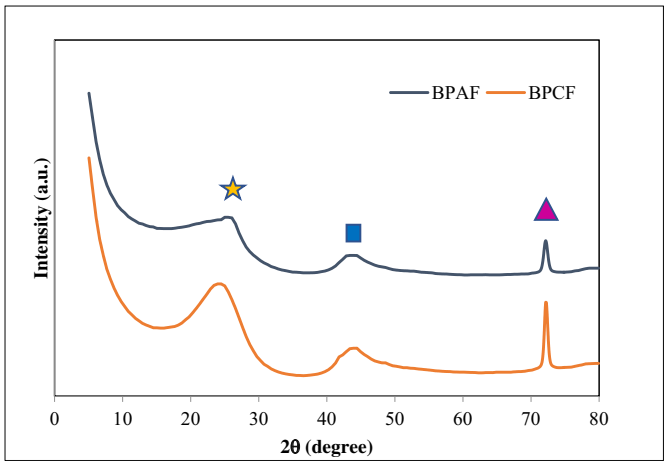

Fig. 4. X-ray diffraction patterns of as-synthesized (BPCF) and activated (BPAF) carbon foams (▲: orthorhombic graphite, ★: hexagonal carbon, ■: hexagonal graphite). (For interpretation of the references to color in this figure legend, the reader is referred to the web version of this article.)

Table 5
XRD parameters of biopitch-based carbon foams.

Foam	2θ (002) (°)	d_{002} (nm)	2θ (100) (°)	d_{100} (nm)
BPCF	23.95	0.3713	43.90	0.2061
BPAF	25.00	0.3559	43.38	0.2084

form of graphite is defined as hexagonal graphite with an ABAB stacking series of the graphene layers. For all that, the irregular parallel stacking of the layers appears generally in the carbonaceous materials synthesized at temperatures below 1300 °C. In such a turbostratic structure, the hexagon layers are generally smaller and only limited layers are stacked in parallel [42].

The (0 0 2) diffraction peaks observed at 2θ = 24° are indicative of the short range of adjacent aromatic rings and lead to the desired distribution of interatomic distances between the carbon atoms. In similar composite materials such as eucalyptus lignin, hardened phenol-formaldehyde resin-based fibers, (0 0 2) peaks can be observed at elevated temperatures around 1400–1500 °C. Observation of the (0 0 2) peak at a low temperature as in a carbonization temperature of 1050 °C; the thermoplastic character of pitch can be associated with the presence of low molecular weight molecules. These two features provide a better structural arrangement in the first stage of heating and thus facilitate the formation of carbon crystals. The reflection of (1 0 0) and (1 0 1) observed in the range of 2θ = 41–45° is the characteristic reflection of the two-dimensional array of carbon layers in graphite-like materials [15,43]. This reflection is also indicative of the formation of two-dimensional clusters by condensation of aromatic rings at operating temperature.

In the literature, XRD patterns of mesophase pitch-based graphite foam [44], mesophase pitch-based carbon foam [43], coal tar pitch-based carbon foam [45] and mesophase pitch-based graphitized carbon foam [26] structures are given. Due to the XRD patterns of carbon foams synthesized using biopitch, the presence of 23° and 43° peaks specific to carbon foams was found to be consistent with the literature.

3.2.4. Nitrogen sorption analysis

The carbon foam can be defined as a carbon matrix containing a certain number of cells. The foam cell structure significantly affects the strength of the carbon foam. However, it has been found that the micro and meso-pore structure in the foam matrix also affects the strength of the carbon foam [46]. The pore structures of carbonized samples in the foam matrix were examined using N_2 adsorption/desorption isotherms at 77 K (Fig. 5). When the adsorption/desorption isotherms were examined, it was determined that the foams had type IV isotherm which includes micro and meso-pores according to IUPAC classification. BET surface areas, pore volumes and average pore sizes of carbon foams were given in Table 6.

According to the surface area results, it was determined that more porous foams were obtained when the softening point of the biopitch used for the production of carbon foam in the high temperature/pressure reactor was high. After activation with potassium hydroxide, it was determined that the surface areas increased to ~716 m^2/g. Pore size distribution graphs of the carbon foam were also given in Fig. 5. When the graphs were examined, it was seen that the non-activated carbon foams had a regular pore size distribution in the meso-pore area and the potassium hydroxide activated foams in the micro-pore region.

3.2.5. Raman studies

The representative Raman spectra of the carbon foams were given in Fig. 6, showing the D-band at ~1345 cm^{-1} due to the breathing mode of aromatic rings and narrower G-band at ~1600 cm^{-1} associated with the bond stretching of sp^2 carbon. D band of activated carbon foam (BPAF) was lower than that of as-synthesized carbon foam (BPCF).

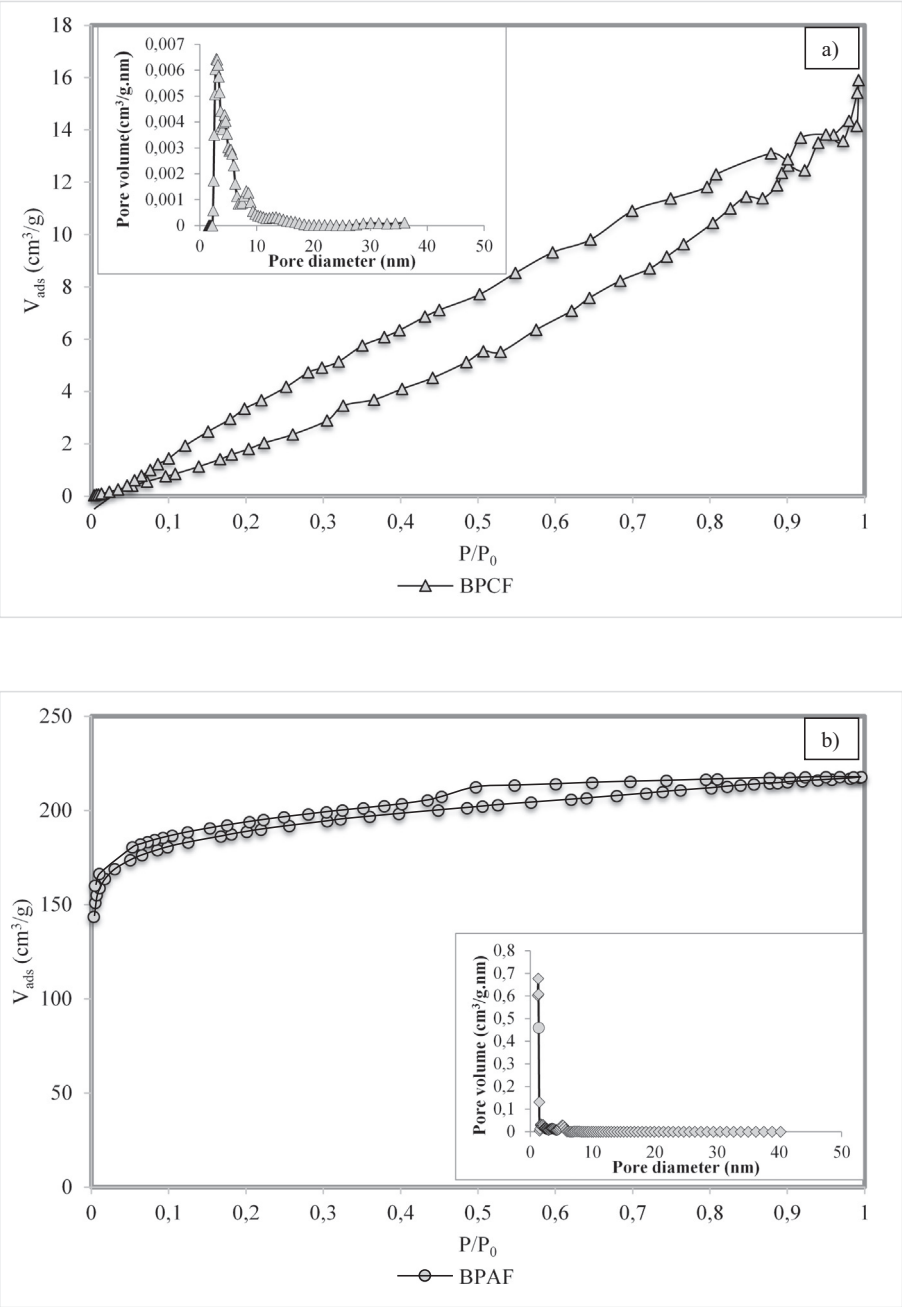

Fig. 5. Sorption isotherms and pore size distribution graphs of a) as-synthesized (BPCF) and b) activated (BPAF) carbon foams.

Table 6
Structural properties of carbon foams produced at 450 °C foaming temperature.

Foam	S_{BET} (m^2/g)	V_{total} (cm^3/g)	V_{micro} (cm^3/g)	V_{meso} (cm^3/g)	Average pore diameter (nm)
BPCF	22,984	0,0211	0	0,0211	2,89
BPAF	715,635	0,3480	0,2919	0,0561	1,29

These indicate the graphitization degree of BPAF was higher than that of BPCF [47]. The intense D-band designates the partial lattice defects through copious pores in proportion to a single graphene layer [48]. From the Raman spectra, it was seen that as-synthesized carbon foam had also G′(2D) and (D + G) bands. The overtone of the D band at 2709 cm^{-1}, denoted as 2D or G′, signifies the defect-free sp^2 carbon. Besides, a broad (D + G) multi-band peaks arisen at ~2941 cm^{-1} are relative with the multi-layer characteristic of graphite [49]. The integrated intensity ratio (ID/IG) of the D and G bands is extensively utilized for characterizing the defect quantity in graphitic materials. The D and D′ bands are defect-induced Raman properties, and hence highly crystalline graphite is not contained these bands [50]. Besides, the possible broadening effect present in the G band is also an indication of the presence of D′ contributions, and it is necessary to perform multiple peak fittings to identify these peaks. The Origin software was operated in the following way to determine peak areas and detect possible D′ band: *i)* the background was subtracted, *ii)* the possible D' band in the G band was deconvoluted, *iii)* the D, G, and 2D peaks were tailored to the Lorentzian function and the D′ peak to the Breit-Wigner-Fano (BWF) line shape function, *iv)* finally, ID/IG ratios were determined from the fitting parameters. Eckmann et al. [51] were focused on defects that are not expected to give D and D' peaks: *i)* charged impurities adsorbed onto the graphene sheet, *ii)* the hopping defects

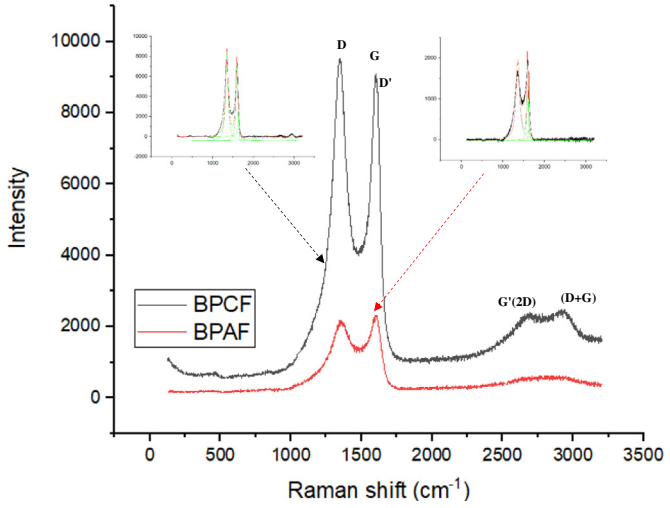

Fig. 6. Raman spectra of as-synthesized (BPCF) and activated (BPAF) carbon foams.

resulting from carbon bond deformation and caused vacancies in graphene, *iii)* on-site defects caused by sp^3 hybridization of out-of-plane atoms and carbon atoms. They stated that hopping and on-site defects were characterized by I(D)/I(D′) ratios of about 10.5 and 1.3, respectively. In addition, in the cause of the formation of non-planar bonds with carbon atoms also causes deterioration in the crystal lattice, it has been stated that a real sp^3 defect comprises of both on-site and hopping defects. According to Fig. 6, ID/IG ratios of as-synthesized (BPCF) and chemically activated (BPAF) carbon foams were found to be 1.86 and 2.23, respectively, while ID/ID' ratios were 0.87 and 0.63. I2D/IG ratios were 0.25 for BPCF and 0.08 for BPAF. According to the results obtained from the Raman spectra, carbon foams were found to be multilayer graphene structure. The results of XRD and Raman spectroscopy analysis were in agreement with each other.

3.2.6. Compressive strength, density and porosity measurement

It is known that the most important parameter affecting the mechanical and thermal conductivity of foams with closed cells is density [52]. The bulk/actual density, porosity and compressive strength of carbonized carbon foams were given in Table 7 and the properties of carbon foams in the literature were given in Table 8. The bulk density of the foams varied between 0.21 and 0.26 g/cm^3 and the actual densities ranged from 1.59 to 1.99 g/cm^3. After the activation of foams with potassium hydroxide, the bulk density decreased, but their actual density increased. Therefore, %porosity value increased by % 7.12 due to increasing porosity as a result of the activation process. The compressive strength of the foams was found to be in the range of 0.40–1.97 MPa.

According to the results of scanning electron microscopy and surface area analysis, it was determined that the porosity increased as a result of activation. While the porosity in the structure of the foams increased, the compressive strength decreased. It is known that the strength of the foam increases when there are a thicker cell wall and shorter cell edge in the structure [46]. The increase in the actual density values measured by the helium gas pycnometer is associated with the formation of a denser sequence due to the development of the cross-linking and aromaticity of the molecules. In addition, as the temperature rises, it is known that the heavier structures of the irregular carbons are formed by the stacking of the planar clusters of the aromatic rings, thus increasing the density [15].

Table 7
The density, porosity and compressive strength of pitch-based carbon foams.

Foam	Strength (MPa)	Bulk density (g/cm^3)	Actual density (g/cm^3)	Porosity (%)
BPCF	1.974	0.2614	1.5850	83.51
BPAF	0.402	0.2104	1.9971	89.46

Table 8
Compressive strength, density and porosity values of carbon foams in the literature.

Foam	Strength (MPa)	Bulk density (g/cm^3)	Porosity (%)	Reference
CTP	6.9–12.8	0.61–0.73	45–75	[38]
MPCF	8.6–10.9	0.34–0.45	–	[53]
CTP	17.79–21.27	0.61–0.76	–	[37]
ECF	0.010	0.005	–	[54]
CF	1.47–3.31	0.24–0.58	37–86	[35]
CF	25.8	0.6	–	[55]
WVU	18.7	0.31	–	[45]
ChSF	17.4	0.59	–	
Ultramet RVC	0.763	0.042	–	[56]
ERG RCV	0.28–0.48	–	–	
Touchstone	15.2–20.7	0.16–0.50	–	
MER	1.7–7.0	0.016–0.62	–	
ORNL	1.0–3.5	0.25–0.65	–	
CF	–	0.64–0.76	45.3–63.8	[57]

4. Conclusion

In this study, an alternative production method for carbon foams, which are widely used in many areas in recent years, has been investigated. It is known that coal tar pitch, petroleum pitch, and mesophase pitch are produced from pyrolysis liquids, which are the by-product of coal and oil processing plants. In the process of producing carbonaceous materials using these pitches, the applied high temperature and pressure processes are both quite difficult and expensive. Compared to these methods, the use of biomass tar pitches and the solvolytic liquefaction process can produce carbon foam by more economical and simpler methods. In this study, as an alternative to pitch-based production methods, spruce tree sawdust, industrial waste, was selected as biomass and carbon foam was produced. In the case of carbon foam production, the foam properties obtained by using the same raw material in the solvolytic liquefaction process are also considered; it is concluded that the properties of the materials can be controlled by adjusting the following parameters:

- Precursor (bio-polyol/bio-pitch)
- Foaming method (solvolysis/high temperature-pressure reaction)
- Reagent type/amount
- Reactor pressure and temperature
- Chemical activation
- Activation temperature

These properties include C content, surface area, porosity, thermal stability, crystal structure, and strength. While carbon foam produced with solvolytic reaction had 62–80% carbon content, biopitch-based carbon foams were found to have higher carbon content as 83–89%. Carbon foam derived from BPCF and BPAF revealed better mechanical properties than resin-based carbon foams. In this respect, the resin-based foam had a maximum compressive strength of 1.08 MPa, while the biopitch-based foam was 82.4% higher. Although the porosity values of the produced foams were higher than the fossil pitch-based foams, they were lower than the foams produced by the solvolytic reaction of the same raw material. In a further aspect, it has been found that the surface area of the pitch-based carbon foams can be increased by the chemical activation process. Thereby it was concluded that by overcoming the limitations encountered in practice and could be addressing more areas. As a result, it is predicted that carbon foams with

regular mesoporous structure and high surface area can be considered as a catalyst support in advanced wastewater treatment technologies or as an adsorbent in liquid- or gas-phase adsorption process.

Supplementary data to this article can be found online at https://doi.org/10.1016/j.diamond.2019.04.032.

References

[1] C. Quan, A. Li, N. Gao, Synthesis of carbon nanotubes and porous carbons from printed circuit board waste pyrolysis oil, J. Hazard. Mater. (2010) 911–917.
[2] P. Jana, V. Fierro, A. Pizzi, A. Celzard, Biomass-derived, thermally conducting, carbon foams for seasonal thermal storage, Biomass Bioenergy 67 (2014) 312–318.
[3] R. Narasimman, K. Prabhakaran, Preparation of low density carbon foams by foaming molten sucrose using an aluminium nitrate blowing agent, Carbon (2012) 1999–2009.
[4] Googin, J., Napier, J. and Scrivner, M., "Method For Manufacturing Foam Carbon Products", United States, Patent No. US 3345440 (1967).
[5] N. Ozbay, A.S. Yargic, Carbon foam production from bio-based polyols of liquefied spruce tree sawdust: effects of biomass/solvent mass ratio and pyrolytic oil addition, J. Appl. Polym. Sci. 136 (11) (2019) 47185.
[6] R. Araújo, V. Pasa, B. Melo, Effects of biopitch on the properties of flexible polyurethane foams, Eur. Polym. J. 41 (6) (2005) 1420–1428.
[7] W.D. Betts, "Tar and Pitch", Kirk-Othmer Encyclopedia of Chemical Technology, John Wiley & Sons, Inc, 2000, pp. 1–2.
[8] W.M. Qiao, M. Huda, Y. Song, S.H. Yoon, Y. Korai, I. Mochida, O. Katou, H. Hayashi, K. Kawamoto, Carbon fibers and films based on biomass resins, Energy Fuel 19 (6) (2005) 2576–2582.
[9] M. Prauchner, V. Pasa, C. Otani, S. Otani, Characterization and thermal polymerization of eucalyptus tar pitches, Energy Fuel 15 (2) (2001) 449–454.
[10] M. Khan, L. Tiehu, T.K. Zhao, Z. Ali, A. Malik, A. Khan, I. Khan, A. Ullah, S. Jiao, M. Idrees, C. Xiong, Effect of multi walled carbon nanotubes and diamond nanoparticles on the structure and properties of carbon foams, Diam. Relat. Mater. 79 (2017) 119–126.
[11] G. Xu, T. Yang, Z. Fang, Q. Wang, C. Yang, X. Zhao, Preparation and characterization of coal-based carbon foams by microwave heating process under ambient pressure, Diam. Relat. Mater. 86 (2018) 63–70.
[12] F.S. Boi, X. Zhang, D. Medranda, Evidence of sp3-rich nano-diamond-like characteristics in amorphous carbon foam continuously filled with α-Fe, Diam. Relat. Mater. 84 (2018) 190–195.
[13] F. Jones, Handbook of Polymer-fibre Composites, Longman Scientific and Technical, Essex, 1994.
[14] R. Gill, Carbon Fibres in Composites Materials, Butterworth Books, London, 1994.
[15] M.J. Prauchner, V.M.D. Pasa, N.D.S. Molhallem, C. Otani, S. Otani, L.C. Pardini, Structural evolution of eucalyptus tar pitch-based carbons during carbonization, Biomass Bioenergy 28 (2005) 53–61.
[16] M. Prauchner, V. Pasa, S. Otani, C. Otani, Biopitch-based general purpose carbon fibers: processing and properties, Carbon 43 (2005) 591–597.
[17] R. Assis, V. Pasa, Blends of phenolic resins with guaiacyl-siringyl units in their structures, Atibaia (1998) 277–281.
[18] J.H. Harker, J.R. Backhurst, Fuel and energy, Academic Press Limited, London, 1981.
[19] J. Rocha, A. Coutinho, C. Luengo, Biopitch produced from eucalyptus wood pyrolysis liquids as a renewable binder for carbon electrode manufacture, Braz. J. Chem. Eng. 19 (02) (2002) 127–132.
[20] J. Wang, S. Kaskel, KOH activation of carbon-based materials for energy storage, J. Mater. Chem. 22 (45) (2012) 23710–23725.
[21] E. Apaydın-Varol, Y. Erülken, A study on the porosity development for biomass based carbonaceous materials, J. Taiwan Inst. Chem. Eng. 54 (2015) 37–44.
[22] Y. Sun, P. Webley, Preparation of activated carbons with large specific surface areas from biomass corncob and their adsorption equilibrium formethane, carbon dioxide, nitrogen, and hydrogen, Ind. Eng. Chem. Res. 50 (2011) 9286–9294.
[23] C. Zhang, W. Song, Q. Ma, L. Xie, X. Zhang, H. Guo, Enhancement of CO_2 capture on biomass-based carbon from black locust by KOH activation and ammonia modification, Energy Fuel 30 (5) (2016) 4181–4190.
[24] B. Petrova, B. Tsyntsarski, T. Budinova, N. Petrov, L.F. Velasco, C.O. Ania, Activated carbon from coal tar pitch and furfural for the removal of P-nitrophenol and M-aminophenol, Chem. Eng. J. 172 (2011) 102–108.
[25] M. Perez, M. Granda, R. Santamaria, T. Morgan, R. Menendez, A thermoanalytical study of the co-pyrolysis of coal-tar pitch and petroleum pitch, Fuel 83 (2004) 1257–1265.
[26] A. Yadav, R. Kumar, G. Bhatia, G. Verma, Development of mesophase pitch derived high thermal conductivity graphite foam using a template method, Carbon 49 (11) (2011) 3622–3630.
[27] B. Tsyntsarski, B. Petrova, T. Budinova, N. Petrov, M. Krzesinska, S. Pusz, J. Majewska, P. Tzvetkov, Carbon foam derived from pitches modified with mineral acids by a low pressure foaming process, Carbon (2010) 3523–3530.
[28] R. Prieto, E. Louis, J. Molina, Fabrication of mesophase pitch-derived open-pore carbon foams by replication processing, Carbon (2012) 1904–1912.
[29] J. Kershaw, K. Black, Structural characterization of coal-tar and petroleum pitches, Energy Fuel 7 (1993) 420–425.
[30] M.J. Prauchner, V.M.D. Pasa, C. Otani, S. Otani, S.M.C. de Menezes, Eucalyptus tar pitch pretreatment for carbon material processing, J. Appl. Polym. Sci. 91 (2004) 1604–1611.
[31] M. Prauchner, V. Pasa, S. Menezes, Solid-state 13C NMR quantitative study of eucalyptus tar pitches, J. Wood Chem. Technol. 21 (4) (2001) 371–385.
[32] B. Melo, V. Pasa, Composites based on eucalyptus tar pitch/castor oil polyurethane and short sisal fibers, J. Appl. Polym. Sci. 89 (14) (2003) 3797–3802.
[33] R. Araújo, V. Pasa, New eucalyptus tar-derived polyurethane coatings, Prog. Org. Coat. 51 (2004) 6–14.
[34] R. Araújo, V. Pasa, Mechanical and thermal properties of polyurethane elastomers based on hydroxyl-terminated polybutadienes and biopitch, J. Appl. Polym. Sci. 88 (2003) 759–766.
[35] A. Eksilioglu, N. Gencay, M. Yardım, E. Ekinci, Mesophase AR pitch derived carbon foam: effect of temperature, pressure and pressure release time, J. Mater. Sci. 41 (2006) 2743–2748.
[36] J. Klett, R. Hardy, E. Romine, C. Walls, T. Burchell, High-thermal-conductivity, mesophase-pitch-derived carbon foams: effect of precursor on structure and properties, Carbon 38 (7) (2000) 953–973.
[37] H. Liu, T. Li, X. Wang, W. Zhang, T. Zhao, Preparation and characterization of carbon foams with high mechanical strength using modified coal tar pitches, J. Anal. Appl. Pyrolysis 110 (2014) 442–447.
[38] X. Wang, J. Zhong, Y. Wang, M. Yu, A study of the properties of carbon foam reinforced by clay, Carbon (2006) 1560–1564.
[39] M. Inagaki, J. Qiu, Q. Guo, Carbon foam: preparation and application, Carbon 87 (2015) 128–152.
[40] P. Kun, F. Wéber, C. Balázsi, Preparation and examination of multilayer graphene nanosheets by exfoliation of graphite in high efficient attritor mill, Cent. Eur. J. Chem. 9 (1) (2011) 47–51.
[41] M. Clugston, R. Flemming, Advanced Chemistry, Chapter 6.4. Delocalization, Oxford University Press, 2000, pp. 88–89.
[42] H. Marsh, F. Rodríguez-Reinoso, Production and reference material, Activated Carbon (2006) 454–508.
[43] M. Wang, C. Wang, T. Li, Z. Hu, Preparation of mesophase-pitch-based carbon foams at low pressures, Carbon 46 (2008) 84–91.
[44] J. Yang, Z. Shen, R. Xue, Z. Hao, Study of mesophase pitch-based graphite foam used as anodic materials in Lithium ion rechargeable batteries, J. Mater. Sci. 40 (5) (2005) 1285–1287.
[45] B. Tsyntsarski, B. Petrova, T. Budinova, N. Petrov, L.F. Velasco, J.B. Parra, C.O. Ania, Porosity development during steam activation of carbon foams from chemically modified pitch, Microporous Mesoporous Mater. (2012) 56–61.
[46] C. Chen, E.B. Kennel, A.H. Stiller, P.G. Stansberry, J.W. Zondlo, Carbon foam derived from various precursors, Carbon (2006) 1535–1543.
[47] S. Li, Y. Tian, Y. Zhong, X. Yan, Y. Song, Q. Guo, L. Liu, Formation mechanism of carbon foams derived from mesophase pitch, Carbon 49 (2) (2011) 618–624.
[48] X. He, N. Zhang, X. Shao, M. Wu, M. Yu, J. Qiu, A layered-template-nanospace-confinement strategy for production of corrugated graphene nanosheets from petroleum pitch for supercapacitors, Chem. Eng. J. 297 (2016) 121–127.
[49] Karthik, M., Faik, A., Doppiu, S., Roddatis, V., D'Aguanno, B. "A simple approach for fabrication of interconnected graphitized macroporous carbon foam with uniform mesopore walls by using hydrothermal method", Carbon, 87: 434–443 (2015).
[50] M.A. Pimenta, G. Dresselhaus, M.S. Dresselhaus, L.G. Cancado, A. Jorio, R. Saito, Studying disorder in graphite-based systems by Raman spectroscopy, Phys. Chem. Chem. Phys. 9 (11) (2007) 1276–1290.
[51] A. Eckmann, A. Felten, A. Mishchenko, L. Britnell, R. Krupke, K.S. Novoselov, C. Casiraghi, Probing the nature of defects in graphene by Raman spectroscopy, Nano Lett. 12 (8) (2012) 3925–3930.
[52] X. Luo, A. Mohanty, M. Misra, Lignin as a reactive reinforcing filler for water-blown rigid biofoam composites, Ind. Crop. Prod. 47 (2013) 13–19.
[53] H. Liu, T. Li, Y. Shi, X. Wang, J. Lv, W. Zhang, Effect of different secondary quinoline insoluble content on thecellular structure of carbon foam derived from coal tar pitch, J. Anal. Appl. Pyrolysis 108 (2014) 310–315.
[54] S. Chen, G. He, H. Hu, S. Jin, Y. Zhou, Y. He, S. He, F. Zhao, H. Hou, Elastic carbon foam via direct carbonization of polymer foam for flexible electrodes and organic chemical absorption, Energy Environ. Sci. 6 (2013) 2435–2439.
[55] S.P. Zhang, M.X. Liu, L.H. Gan, F.R. Wu, Z.J. Xu, Z.X. Hao, L.W. Chen, Synthesis of carbon foams with a high compressive strength from arylacetylene, New Carbon Mater. 25 (1) (2010) 9–14.
[56] N. Gallego, J. Klett, Carbon foams for thermal management, Carbon 41 (2003) 1461–1466.
[57] W. Li, H. Zhang, X. Xiong, F. Xiao, A study of the properties of mesophase-pitch-based foam/graphitized carbon black composites, Mater. Sci. Eng. A 528 (6) (2011) 2999–3002.